Anomaly Detection in Bridges Using Interferometric Synthetic Aperture Radar (InSAR)

OTHMANE LASRI, ELEONORA CLEMENO
and MARIA PINA LIMONGELLI

ABSTRACT

Structural Health Monitoring (SHM) plays a crucial role in supporting decision-makers by providing vital information on the structural integrity of bridges. Traditional SHM systems typically rely on in-situ sensors, which can be time-consuming to install and vulnerable to failure during extreme weather events. In contrast, Synthetic Aperture Radar Interferometry (InSAR), leveraging active radar sensors mounted on satellites, has emerged as a promising remote sensing alternative. This technique enables the monitoring of any structure visible from the satellite's orbit, eliminating the need for on-site sensor installation. Furthermore, depending on the availability of satellite imagery, InSAR allows for retrospective analysis of structural behavior. Historical displacement data can be used to detect anomalous trends, potentially serving as an early warning for hazardous structural conditions. This paper presents an anomaly detection procedure based on InSAR displacement time series. The proposed method is applied to a riverine bridge that collapsed in 2023. The displacement datasets are sourced from the European Ground Motion Service (EGMS), which utilizes Sentinel-1 satellite imagery.

1. INTRODUCTION

Bridges and viaducts play a crucial role in road networks. Their reduced functionality or collapse can strongly impact the economy and safety of entire communities [1]. Several bridge collapses in recent years have shown the societal economic impact of bridge closures resulting for example from increased travel distances [1], beyond the direct cost of collapse [2]. Due to the aging of those infrastructures and the increase in traffic demand, structural degradation of bridges is becoming a crucial problem. Design errors, construction mistakes, natural hazards, collision, and overload are the top five leading causes of bridge failures, resulting in more than 70% of bridge failures [3]. Furthermore, leading to flood-induced scour which is one of main causes of riverine bridge collapse [3]. In this context, Structural Health Monitoring systems (SHMs) provide valid resources to decision-makers. P. Clemente shows how a proper maintenance plan combined with a monitoring strategy, could have provided in advance valuable information about the operational state of the Polcevera bridge [2]. Technological evolution has made available a wide choice of SHM devices and algorithms [4]. Despite the advantages provided by in-situ SHM systems, their widespread adoption is limited by skepticism of owners and decision-makers primarily linked to the up-front cost they have to sustain without a consistent estimation of the benefit they bring. Recently, due to the development of advanced Differential InSAR (DInSAR) algorithms and the increase in the temporal and spatial resolution of SAR images, InSAR technology can provide low-cost measurement of deformations of human artefacts like bridges and viaducts [5–7]. However, despite several studies have shown the capability of InSAR in detecting collapse precursors displacement patterns, anomaly detection procedures based on InSAR time series remain undeveloped. The aim of this paper is to provide an anomaly detection strategy based on the InSAR time series. In the remainder of this paper, Section 2 presents the principles of InSAR, Sections 3 and 4 introduce the methodology and the case study, respectively. The results are presented in Section 5, and the conclusions are provided in Section 6.

2. INSAR PRINCIPLES

SAR satellites are active devices that irradiate electromagnetic waves at different bands of the microwave domain towards a certain area of interest or target. A fraction of the signal is backscattered and returned to the sensor, where amplitude and phase are recorded. The amplitude of the backscattered signal depends on the amount of electromagnetic backscattered energy which depends on acquisition geometry, radar carrier frequency, radar resolution, wavelength and polarization, size of the scatterers, surface roughness and orientation [8]. Signals backscattered from exposed rocks and urban areas show strong amplitudes, whereas smooth flat surfaces (like water basins) backscatter low amplitude signals. The phase of the signal is proportional to the target-sensor distance. In the ideal case where the phase is correlated only to the target-sensor distance, analyzing phase variations among two radar images of the same area of interest can inform about the area movement. Based on this concept, DInSAR techniques aim at obtaining the deformation rate of the target by analysing radar images acquired over the same area at different times. However, the signal phase is also affected by atmospheric pressure, water vapour and soil moisture [9,10] may alter the quantification of the distance. Furthermore, decorrelations linked to errors in satellite orbit and surface elevation determination limit the use of the phase difference between two images to assess the target displacement. Accounting for all these factors, the phase change among two images can be described as follows [11]:

$$\Delta\varphi_i = \frac{4\pi}{\lambda}\Delta r_{Ti} + \Delta\alpha_i + \Delta n_i + \varepsilon_{topo,i} \quad (1)$$

Δr_{Ti} represents the phase change due to the movement in the Line of Sighr (LOS) direction, $\Delta\alpha_i$ the atmospheric phase contribution, Δn_i the decorrelation noise and $\varepsilon_{topo,i}$ is the phase contribution due to possible errors in the Digital Elevation Model (DEM). The main challenge of DInSAR techniques is to assess the phase change Δr_{Ti} removing or reducing the effect of the other parameters. To address this challenge, advanced (or Multi-Temporal) DInSAR techniques have been developed over the past decades, supported by the growing availability of SAR satellites with diverse footprint sizes, acquisition modes, bandwidths (typically X-, C-, and L-band), and revisit times. These methods enable the accurate monitoring of surface displacements over time reducing the uncertainty by computing the phase difference between several couples of images. They produce displacement time series and mean deformation velocity maps achieving up to sub-centimeter accuracy depending on the type of sensor and relevant bandwidth. The European Space Agency (ESA) has recently launched the European Ground Motion Service (EGMS) as part of the Copernicus program. Operational since 2022, EGMS utilizes MT-DInSAR techniques combined with GNSS calibration, providing user-friendly services through a dedicated portal with annual updates. It processes data collected by the Sentinel-1 constellation, which consists of two twin satellites operating in the C-band.

3. ANOMALY DETECTION

The process used for anomaly detection involves the computation of the time histories of the 'representative' displacements [12], the computation of the expected displacements in reference conditions, based on a regression model and the anomaly detection based on control charts. The Measurement Points (MPs) provided by satellites acquisitions are generally distributed on the structure in a non-uniform way. To use these measurements for the analysis of the structural condition, the MPs are grouped into zones. The displacement of each zone is calculated as the average of the LOS displacements of the MPs within that zone. Using average MPs time series from the ascending and descending tracks and neglecting the displacements along the North-South direction, the Up and East deformation components can be estimated using the following relationships [7].

$$\begin{bmatrix}\delta_{LOS,A}\\ \delta_{LOS,D}\end{bmatrix} \cong \begin{bmatrix}C_{E,A} & C_{U,A}\\ C_{E,D} & C_{U,D}\end{bmatrix}\begin{bmatrix}\delta_E\\ \delta_U\end{bmatrix} \tag{2}$$

where $\delta_{LOS,A}$ and $\delta_{LOS,D}$ represent the LOS displacements measured from ascending and descending tracks, respectively. $C_{E,A}$ and $C_{E,D}$ represent the cosines of the angle between the East and LOS direction, and $C_{U,A}$ and $C_{U,D}$ are the cosines of the angle between the Up and LOS direction for each track. The expected displacements in reference condition are computed through a regression model built considering the displacement changes in the longitudinal direction due to temperature in the reference condition. Following reference [13] in this study, a linear regression model is used to represent the relationship between temperature and displacement (dependent variable). A training period is defined to identify the regression model for the reference displacement. This model is then used to predict expected displacements based on temperature data. The regression equation is shown in Equation (3), where y is the displacement vector for the training period, Z is the matrix of the temperatures and β is the unknown vector that offers the relationship between the two variables. The vector ε is included to simulate the variability of the data due to uncertainties connected to the measurements and to the process to extract displacement time histories from InSAR data. This noise represents random variations of the data, with a distribution that follows a normal distribution.

$$y = Z \cdot \beta + \varepsilon \tag{3}$$

The main goal of regression analysis is to estimate the vector β that best fits the observed data based on the independent variable. This is typically done using the least squares method, which minimizes the sum of squared errors[13]. Using this approach, the estimated parameters $\hat{\beta}$ are calculated with the Equation (4):

$$\hat{\beta} = (Z^T Z)^{-1} Z^T \cdot y \tag{4}$$

Once the vector $\hat{\beta}$ has been obtained, using data relating to the training period, the formula (3) can be used to calculate the predicted displacements, using measured temperature values. A Control Chart is applied to the residual E between actual and predicted displacements and defined as the absolute value of their difference, as shown

in Equation (4), where $\delta_{E,M}$ and $\delta_{E;P}$ denote respectively the measured and predicted displacements obtained from the regression model previously described.

$$E = \left|\delta_{E,M} - \delta_{E;P}\right| \tag{5}$$

The T^2 statistic is calculated using Equation (6) [13], where $\bar{\bar{E}}$ represents the average of residuals over the past r observations, $\bar{\bar{E}}$ is the average of residuals when the process is under control, and S is the covariance matrix of the process, estimated based on the actual displacement vector $\delta_{E;P}$ over the reference period.

$$T^2 = r\left(\bar{E} - \bar{\bar{E}}\right)^T S^{-1}\left(\bar{E} - \bar{\bar{E}}\right) \tag{6}$$

The normal variability of the structural condition is defined by the range between the Lower Control Limit (LCL) and the Upper Control Limit (UCL). Since the T^2 statistic is always positive, the LCL is assumed to be zero. The UCL, instead, is defined as the critical values for 5% observations.

4. THE CASE STUDY

The Ortiano 2 Viaduct, commonly known as the Longobucco Bridge, is located along State Road 117 "Sila-Mare." crossing the Trionto River with the axis approximately oriented from West to East. The bridge was inaugurated in 2015 to improve connections between the Sila Plateau and the Ionian coast. However, the viaduct suffered a structural collapse on May 3, 2023, only nine years after its opening. The bridge extends in an almost east-west direction, measuring approximately 210 meters in length and 10 meters in width (see Figure 1). The bridge was designed with prestressed reinforced concrete beams supported by six piers of varying heights. Publicly available information about the bridge's detailed dimensions or structural design is limited. However, based on the analysis of images available online, it can be inferred that the beams were simply supported by the piers. According to news reports, early signs of failure were observed as early as November 2022. The final collapse occurred at the joint between the third and fourth spans and was triggered by the flooding of the Trionto River, following heavy rainfalls in the region. The analysis in this study focuses on detecting differential displacements of the bridge, monitored using Sentinel-1 satellite data from 2018 to 2022. The study aims to identify any signs of structural anomalies in the years before the collapse.

Figure 1: The Longobucco Bridge

5. RESULTS

In this study, the InSAR data provided by the European Ground Motion Service (EGMS) portal are used combining displacements retrieved from ascending (ASC) and descending (DESC) tracks. Sentinel 1 data from 03/01/2018 to 31/12/2022 are used in this study. The MPs are organized on two zones, namely Zona A and Zona B. Combining the displacements from the ascending and descending tracks, the displacements in the Up (vertical) and East (approximately longitudinal) bridge displacements are estimated. The analysis concentrates on longitudinal (East) displacements on which seasonal deformation effects are typically more pronounced [6]. Longitudinal displacements are estimated using the procedure described in section 3. In Figure 2 The triangles indicate MPs from ASC track, the squares MPs from the DESC track, respectively. In Figure 3 the West-East displacement of Zone A (in red) and Zone B (in blue) are plotted. The displacement predicted using equation (3), considering a 10% Gaussian noise is indicated by the dashed line. The measured displacement is indicated by the solid line. Both Zone A and Zone B exhibit a deviation of the predicted with respect to the measured displacement. However, the deviation starts in May 2022 for Zone A and approximately one year before, in May 2021, for Zone B.

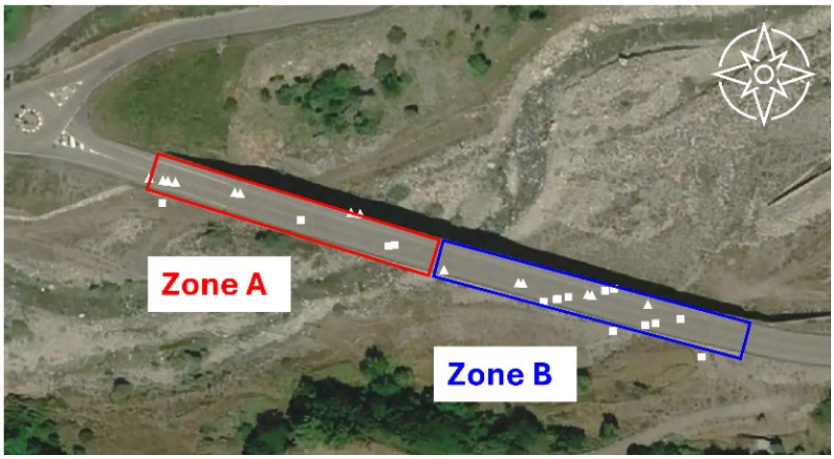

Figure 2: Clustering of MPs in two zones.

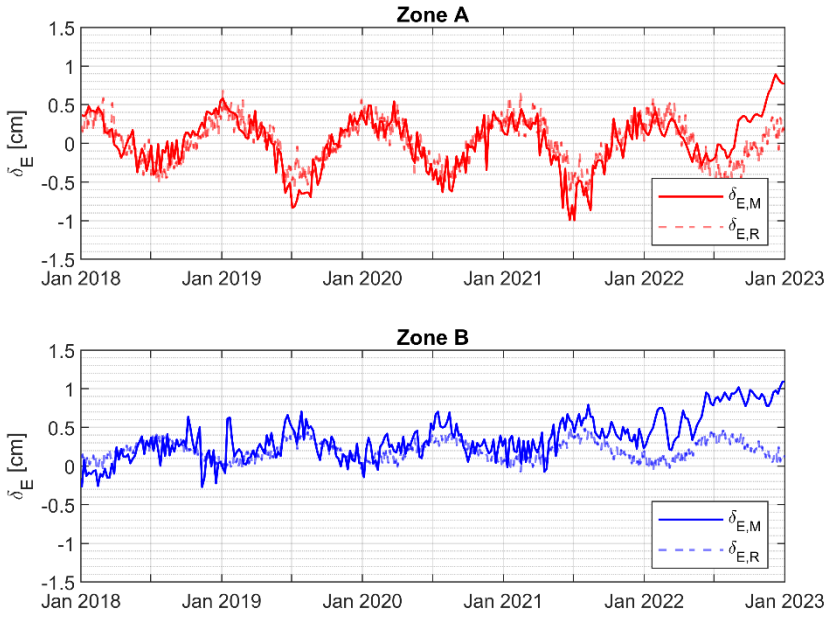

Figure 3: The West-East displacement time sheets of the two zones defined on the bridge.

This is more clearly shown by the residuals reported in in Figure 4. Figure 5 shows the control chart used for anomaly detection. The blue vertical lines indicating heavy rain occurred, which could have potentially increased the hydraulic load on the bridge substructures. Starting from October 2021, several T^2 values exceed the threshold, suggesting an anomalous behavior. An analysis of the most significant rainfall events showed that in October 2021, there was a heavy rain event.

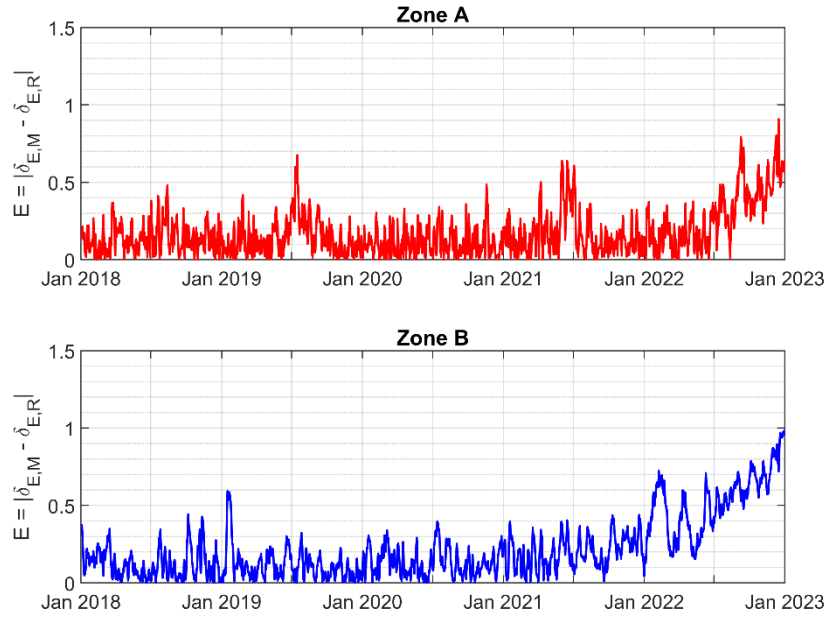

Figure 4: The red line shows residual time series of zone A, the blue line shows the residual time series of zone B.

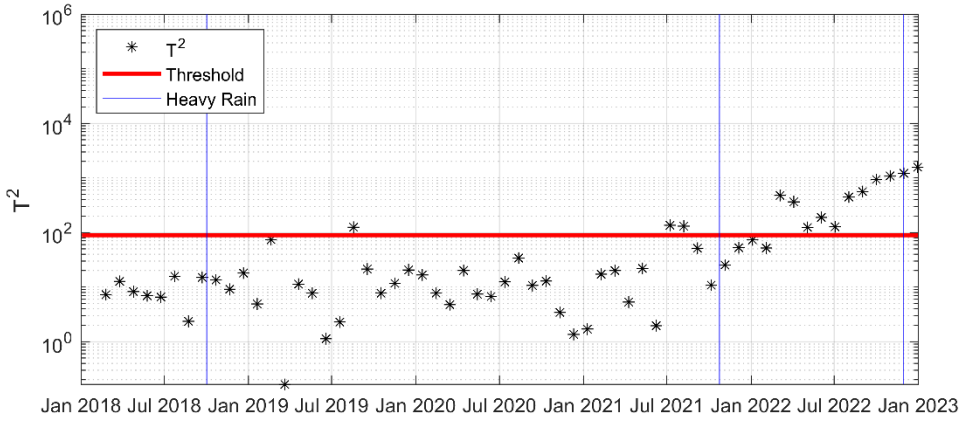

Figure 5: Control chart with a threshold corresponding to the upper 5% of observations.

6. CONCLUSIONS

In this paper, an anomaly detection procedure based on InSAR is applied to identify pre-collapse anomalies in the Longobucco Bridge in Italy, which collapsed on May 3, 2023, during a flood event involving the Trionto River. The proposed methodology employs linear regression to model the bridge's longitudinal displacements as a function of temperature. The residuals—i.e., the differences between the predicted and observed displacements—are used as damage indicators. A T^2 control chart is introduced as the statistical detection tool. The results indicate that certain areas of the bridge exhibited anomalous displacement trends several months prior to the collapse. Notably, the residuals between the predicted and actual displacements began to increase well before the failure event. It is important to acknowledge that this study is based on a low-resolution InSAR dataset, which provides a limited number of MPs on the structure. More precise analyses using high-resolution SAR imagery, in conjunction with physics-based modeling, would enable a more detailed assessment and more robust conclusions regarding the collapse mechanism. Despite these limitations, the study demonstrates the potential of open-access InSAR data for preliminary anomaly detection in riverine bridges. This approach could serve as a valuable early warning tool to support infrastructure risk management.

7. ACKNOWLEDMENT

This study was carried out within the RETURN Extended Partnership and received funding from the European Union Next-GenerationEU (National Recovery and Resilience Plan – NRRP, Mission 4, Component 2, Investment 1.3 – D.D. 1243 2/8/2022, PE0000005).

8. REFERENCES

[1] B. Kim, S. Shin, D. Kim, Scenario-Based Economic Impact Analysis for Bridge Closures Due to Flooding: A Case Study of North Gyeongsang Province, South Korea, Water (Basel) 10 (2018) 981. https://doi.org/10.3390/w10080981.

[2] P. Clemente, Monitoring and evaluation of bridges: lessons from the Polcevera Viaduct collapse in Italy, J Civ Struct Health Monit 10 (2020) 177–182. https://doi.org/10.1007/s13349-020-00384-6.
[3] G. Zhang, Y. Liu, J. Liu, S. Lan, J. Yang, Causes and statistical characteristics of bridge failures: A review, Journal of Traffic and Transportation Engineering (English Edition) 9 (2022) 388–406. https://doi.org/10.1016/j.jtte.2021.12.003.
[4] Y. Yang, Y. Zhang, X. Tan, Review on Vibration-Based Structural Health Monitoring Techniques and Technical Codes, Symmetry (Basel) 13 (2021) 1998. https://doi.org/10.3390/sym13111998.
[5] S. Selvakumaran, S. Plank, C. Geiß, C. Rossi, C. Middleton, Remote monitoring to predict bridge scour failure using Interferometric Synthetic Aperture Radar (InSAR) stacking techniques, International Journal of Applied Earth Observation and Geoinformation 73 (2018) 463–470. https://doi.org/10.1016/j.jag.2018.07.004.
[6] E. Farneti, N. Cavalagli, M. Costantini, F. Trillo, F. Minati, I. Venanzi, F. Ubertini, A method for structural monitoring of multispan bridges using satellite InSAR data with uncertainty quantification and its pre-collapse application to the Albiano-Magra Bridge in Italy, Struct Health Monit 22 (2023) 353–371. https://doi.org/10.1177/14759217221083609.
[7] V. Macchiarulo, P. Milillo, C. Blenkinsopp, C. Reale, G. Giardina, Multi-temporal InSAR for transport infrastructure monitoring: recent trends and challenges, Proceedings of the Institution of Civil Engineers - Bridge Engineering 176 (2023) 92–117. https://doi.org/10.1680/jbren.21.00039.
[8] R.F. Hanssen, Radar Interferometry, Springer Netherlands, Dordrecht, 2001. https://doi.org/10.1007/0-306-47633-9.
[9] A. Ferretti, A. Monti-Guarnieri, C. Prati, F. Rocca, InSAR Principles: Guidelines for SAR Interferometry Processing and Interpretation (TM-19, February 2007), The Netherlands, 2007.
[10] D. Cusson, K. Trischuk, D. Hébert, G. Hewus, M. Gara, P. Ghuman, Satellite-Based InSAR Monitoring of Highway Bridges: Validation Case Study on the North Channel Bridge in Ontario, Canada, Transportation Research Record: Journal of the Transportation Research Board 2672 (2018) 76–86. https://doi.org/10.1177/0361198118795013.
[11] A. Ferretti, C. Prati, F. Rocca, Permanent scatterers in SAR interferometry, IEEE Transactions on Geoscience and Remote Sensing (2001). https://doi.org/10.1109/36.898661.
[12] P.F. Giordano, Z.I. Turksezer, M. Previtali, M.P. Limongelli, Damage detection on a historic iron bridge using satellite DInSAR data, Struct Health Monit 21 (2022) 2291–2311. https://doi.org/10.1177/14759217211054350.
[13] F. Magalhães, A. Cunha, E. Caetano, Vibration based structural health monitoring of an arch bridge: From automated OMA to damage detection, Mech Syst Signal Process 28 (2012) 212–228. https://doi.org/10.1016/j.ymssp.2011.06.011.